XTRAFFIC: A DATASET WHERE TRAFFIC MEETS INCIDENTS WITH EXPLAINABILITY AND MORE

Anonymous authors
Paper under double-blind review

ABSTRACT

Long-separated research has been conducted on two highly correlated tracks: traffic and incidents. Traffic track witnesses complicating deep learning models, e.g., to push the prediction a few percent more accurate, and the incident track only studies the incidents alone, e.g., to infer the incident risk. We, for the first time, spatiotemporally aligned the two tracks in a large-scale region (16,972 traffic nodes) over the whole year of 2023: our XTraffic dataset includes **traffic**, i.e., time-series indexes on traffic flow, lane occupancy, and average vehicle speed, and **incidents**, whose records are spatiotemporally-aligned with traffic data, with seven different incident classes. Additionally, each node includes detailed physical and policy-level meta-attributes of lanes. Our data can revolutionalize traditional traffic-related tasks towards higher interpretability and practice: instead of traditional prediction or classification tasks, we conduct: (1) post-incident traffic forecasting to quantify the impact of different incidents on traffic indexes; (2) incident classification using traffic indexes to determine the incidents types for precautions measures; (3) global causal analysis among the traffic indexes, meta-attributes, and incidents to give high-level guidance of the interrelations of various factors; (4) local causal analysis within road nodes to examine how different incidents affect the road segments' relations. The dataset is available at `https://anonymous.4open.science/r/XTraffic-E069`.

1 INTRODUCTION

In today's era of deep learning, a technological foundation has been laid for intelligent transportation systems (Yu et al., 2018; Zheng et al., 2020; Liu et al., 2022a). Primarily, conducting myriad traffic analysis relies on two types of data: traffic and incident data. Traffic data encompasses the traffic state-related time-series, e.g., volume, speed, and occupancy rate on the road network over time. This continuous stream of data is essential for forecasting the future volume, understanding peak usage times, and optimizing traffic signals and routes (Guo et al., 2021; Li et al., 2022). Real-time traffic data allows for dynamic adjustments to be made, enhancing the efficiency of traffic flow and reducing overall travel times. On the other hand, incident data includes information about traffic accidents, road closures, and unexpected events that can significantly affect traffic flow. This data helps in understanding the impact of such incidents on traffic congestion and travel time, facilitating more accurate predictions and enabling timely responses from traffic management systems (Li et al., 2018a; Lin & Li, 2020). By analyzing patterns and frequencies of incidents, predictive models can also be developed to foresee potential hotspots and prevent future occurrences.

However, current research has been conducting the two tracks of traffic and incident separately, ignoring the inseparable relation of traffic and incident. For example, abundant works (Shao et al., 2022; Lan et al., 2022; Fang et al., 2021; Zhu et al., 2021) have been using various **traffic-only** datasets such as PEMS (Song et al., 2020), META-LA (Song et al., 2020), LargeST (Liu et al., 2024) for traffic forecasting. They achieved relatively high accuracy because, under normal circumstances, traffic flow generally follows a strong regular temporal pattern. However, they ignore that unexpected incidents will cause abnormal and irregular patterns

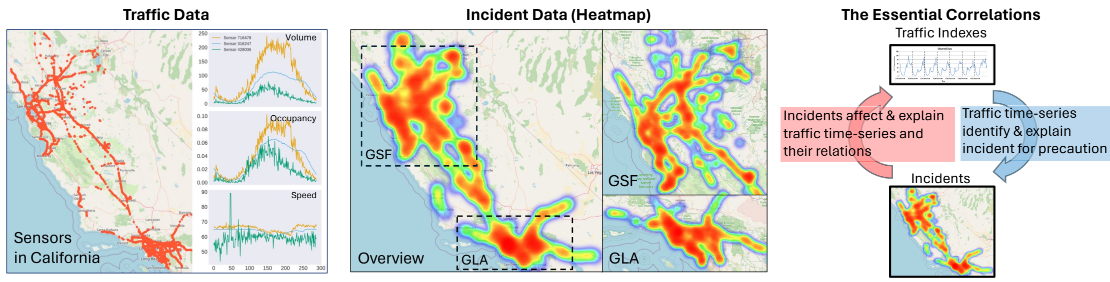

(a) Sensors locations of traffic data, with 3 sensors' volume, occupancy rate, and speed indexes

(b) Incident frequency heatmap, with seven incidents: `1141`, `Fire NoInjure`, `UnknownInjure`, `Hazard`, `AnimalHazard`, `CarFire`

(c) The long-ignored relations of traffic and incident are vital for more explainable and critical analysis

Figure 1: Our XTraffic contains (a) traffic data with road-level meta features, (b) incident data, and (c) their essential yet neglected relations

in traffic flows. On the contrary, in the **incident-only** data (Andersen & Torp, 2018; Moosavi et al., 2019), studies have been done on offering descriptive analysis on the incident patterns (Li et al., 2013; Alsahfi, 2024), predicting the accident risk (Shi et al., 2021), time-to-accident (Anjum et al., 2022), or next incident (Huang et al., 2023), yet there is very limited research using the traffic time-series to identify and explain the incidents and their causal relations with the traffic systems and roads. Moreover, existing open-source accident datasets (Department, 2024; of Motor Vehicles, 2023; of Transport, 2016; Huang et al., 2023) are quite constrained: they only include features related to accidents and lack traffic data for corresponding areas. Additionally, the data granularity is large, and there is no specific location information, such as coordinates or absolute postmile (Abs PM) markers. These factors make conducting related research particularly challenging. Some traffic studies that incorporate incident data use datasets that have not been aggregated or made open source, making it difficult to use them as a standard for evaluating new methods. Additionally, due to the issue of large granularity, it's impossible to analyze the specific impact of accidents on precise road segments. Instead, incident data can only be used to predict general volume within a certain area.

Contributions. To address the research gaps, we introduce the XTraffic dataset. This dataset not only includes three distinct types of traffic time series data for the entire year of 2023 (in Fig. 1(a)), but also encompasses comprehensive incident data (in Fig. 1(b)) and meta-features of roads closely related to traffic flow. The contributions of this dataset can be summarized as follows: (1) We provide a comprehensive collection of multi-type incident records with 476,766 samples, enabling the training and evaluation of traffic forecasting models across various scenarios/incidents. This also supports tasks such as incident discovery and traffic anomaly detection by providing ground truth data. (2) We offer a rich collection of physical and policy-level road meta-features. These features are instrumental for causal analysis of traffic and support the increasingly popular field of interpretable deep learning models. By incorporating these detailed attributes, researchers can delve deeper into the underlying mechanisms that influence traffic behaviors and model predictions. As shown in Fig. 1(c), our XTraffic helps not only **Incident** $\rightarrow$ **Traffic**: e.g., to analyze how incidents affect the traffic states (with our post-incident traffic forecasting in Sec. 4.2) and traffic node relations (local causal analysis in Sec. 4.5), but also **Traffic** $\rightarrow$ **Incident**: e.g., to identify the incidents (incident classification in Sec. 4.3) and explain the incident with other factors from the system (global causal analysis in Sec. 4.4).

To our knowledge, our XTraffic is the most recent in terms of the collection period and contains the largest number of sensors, covering three distinct types of traffic volume. This ensures the timeliness of traffic research, providing a robust foundation for studies aiming to capture and explain traffic dynamics, causation, and interrelations. XTraffic serves as a rigid testing bed and empirical support to justify model effectiveness and interoperability in deep learning and traffic community.

2 Related Work

2.1 Related Work of Traffic and Incident Datasets

Traffic Dataset. Traffic dataset are commonly used in traffic analysis and forecasting as experimental benchmarks. We introduce the existing four public datasets widely leveraged in traffic forecasting experiments. The PeMSD7(M) and PeMSD7(L) are proposed by (Yu et al., 2018). METR-LA and PEMS-BAY(Li et al., 2018b) covered similar regions in California with multiple traffic. However, these datasets are limited to one collection region, our XTraffic instead covers the majority of Metropolitan regions of California including greater San Francisco, San Jose, and Greater Los Angeles. The PEMS03,04,07 and 08 are proposed by (Song et al., 2020). This dataset encompasses four different regions, with data collected using the same rules, supporting multi-region research for traffic analysis and forecasting. Compared to previous datasets, LargeST (Liu et al., 2024) extends both temporally and spatially and includes some basic meta-features. However, these datasets still lack important features such as incidents that significantly impact traffic, as well as road meta-features related to physics and policy. Our XTraffic is the first dataset as such that spatiotemporally align traffic dynamics and traffic incidents, enabling uncomparable potentials for explainable and interpretable traffic management tasks.

Incident Dataset. Incident datasets support the traffic analysis, like the incident impact on traffic, and incident detection. (Huang et al., 2023) proposes a dataset that includes accident data with accident relative features, like accident reason. (Yeddula et al., 2023) also leverages a large accident dataset including various types for accident hotspot prediction. However, limited to the absence of traffic time series, it is hard to do a deeper impact analysis of accidents on traffic based on these datasets. (Lin & Li, 2020) leverages a dataset that includes 13,338 accident records with the traffic flow. However, the dataset is small and non-public. (Zhu et al., 2021) proposes a new accident prediction model based on a dataset with accidents and traffic flow. However, the dataset is not public, either.

2.2 Traffic and Incident Analysis

Traffic Forecasting with Incidents Considered. A large number of works, e.g., STGCN (Yu et al., 2018), STGODE (Choi et al., 2022), DSTAGNN(Lan et al., 2022), are proposed to improve the prediction accuracy based on GNN (Wu et al., 2020) and RNN (Ramakrishnan & Soni, 2018) models. However, these works only consider historical traffic for future traffic, yet other critical impacts, e.g., incidents and meta-features are ignored ((Yuan & Li, 2021; Jiang & Luo, 2022; Tan et al., 2023; Liu et al., 2024) offer detailed reviews in traffic forecasting). There are a few works that have considered incidents when predicting, whose main design is incorporating incident-related embedding as auxiliary information into traditional spatiotemporal prediction framework (Xie et al., 2020; Golze et al., 2021; Liu et al., 2022b; Hong et al., 2024). For example, DIGC-Net (Xie et al., 2020) inputs the type and duration of the incident to predict the affected speed. Yet, the dataset only brings one week of incident data (17-24 Apr 2019) from a small district, being spatiotemporal limited; STCL (Liu et al., 2022b) introduced two-month New York City *Vehicle* incident data as one-hot accident embedding into the prediction of the *Taxi* and *Bike* data. Like what we have observed in most works that analyze traffic with incidents (Liu et al., 2022b; Hong et al., 2024), **the transport modes of traffic data and that of incident data are NOT seamlessly matched**; thus, it will be less convincing to analyze vehicle incidents' impact on bike traffic (bike lane is separated from vehicle lane) or on taxi traffic (taxi is only a subset mode of the whole vehicle). Our XTraffic is the first and only dataset that is (1) spatially and temporally large-scale, (2) that modes in traffic and incident are seamlessly matched (all vehicles), which guarantees unbiased analysis between the traffic and incident.

Incident Classification. It is a crucial task in analyzing non-recurrent congestion (Li et al., 2018a). Recently, several studies have utilized traffic flow data for incident classification (Lin & Li, 2020; Zhu et al., 2021). However, these studies often face at least one of the following three challenges: (1) Small Data Size (Lin & Li, 2020): Many studies suffer from limited datasets that fail to capture the diversity and complexity of traffic patterns, affecting model reliability and generalizability. (2) Limited Dimensionality without Traffic Volume Data (Huang et al., 2023; Yeddula et al., 2023): The absence of critical data dimensions, such as traffic volume, restricts the depth and accuracy of incident classification models. (3) Experiments Based on Non-Public Dataset (Zhu et al., 2021; Lin & Li, 2020): Reliance on proprietary datasets impedes the ability of the broader research community to verify, replicate, or enhance the findings, limiting collaborative advancements.

Traffic Causal Analysis. This task aims to learn the causal structures among different entities in a traffic system. Usually, the causal structures are formulated as Bayesian networks or DAGs (Zheng et al., 2018), where a directed edge denotes the causal link. In the traffic domain, given the traffic indexes are time-series and others can be scalers (e.g., static meta-features), a special DAG structure learning based on heterogeneous data is needed (Lan et al., 2023; 2024). **To learn the global relation of various factors**, e.g., traffic flow, meta-attributes, weather, etc., where each DAG node is a factor to be considered, MultiFun-DAG (Lan et al., 2024) views multivariate time-series in traffic as a multi-function and formulate the structure learning as a "self-expression problem", i.e., $\mathbf{X} = \mathbf{W}\mathbf{X} + \mathbf{Z}$, based on function-to-function regression and the directed acyclic regularization on the coefficients $\mathbf{W}$ (Zheng et al., 2018), a DAG is constructed based on $\mathbf{W}$. MM-DAG (Lan et al., 2023) further consider multi-location at the same time. **To learn local causal relation among different locations**, where each DAG node is a spacial location, DBGCN (Luan et al., 2022) and DCGCN (Lin et al., 2023) combines DAG with GCN, DCGCN further considers the causal links across the time, i.e., node 1 at t_1 affects the node 2 at t_3, and the dynamics of DAG changing over time. The preliminary of these four intended tasks are introduced in Appendix A.4.

3 XTRAFFIC DATACUBE

3.1 COMPARISON WITH EXISTING DATASETS

Table 1: The comparison of Existing Traffic Dataset and XTraffic. Each row represents the largest subset within the corresponding dataset.

Dataset	Nodes	Edges	Slot (Min)	Location	Context	Physics	Policy	Granules	Incdt.
PeMSD7(L)	1,026	14,534	5	✓	✓	-	-	Road	
METR-LA	207	1,515	5	✓	-	-	-	Road	-
PEMS-BAY	325	2,369	5	✓	-	-	-	Road	-
PEMS07	883	865	5	-	-	-	-	Road	-
CA	8,600	201,363	15	✓	✓	-	-	Road	-
XTraffic	16,972	870,100	5	✓	✓	✓	✓	Lane	✓

Table 2: The comparison of Incidents Dataset and XTraffic. We are the only ones who combine traffic with incidents.

Dataset	Incident	Granules	Volume	Speed	Occupancy
CTC (Department, 2024)	1	Point	-	-	-
NYC Col (of Motor Vehicles, 2023)	1	Road	-	-	-
NYS Crashes (Department, 2022)	1	Point	-	-	-
UKA (of Transport, 2016)	1	Point	-	-	-
TAP (Huang et al., 2023)	1	Road	-	-	-
TAA (Bedane, 2020)	1	Road	-	-	-
XTraffic	7	Point	✓	✓	✓

(1) **Base Features Comparison**. In Table 1, we introduce the existing four public datasets widely leveraged in **traffic analysis**. The PeMSD7(M) and PeMSD7(L) are proposed by (Yu et al., 2018). The PEMS03,04,07 and 08 are proposed by (Song et al., 2020). The large-scale traffic dataset LargeST which includes CA, GLA, GBA, and SD subdatasets are proposed by (Liu et al., 2024). We compared the datasets from 7 aspects: Scale (Number of Sensors/Nodes and Neighbors/Edges), Location (Latitude, Longitude, Abs PM), Context (Road Name, City, County), Physics Meta Feature (Road Width, Terrain, Surface Material, etc.), Policy meta feature (Design Speed Limit, Population, Functional Class etc.), Granularity (timer interval, sensor level) and Incident features. As shown in Table 1, our XTraffic is larger than the existing datasets, with 16,972 nodes and 870,100 edges. Compared to other datasets, we include two types of meta features: physics meta feature and policy meta feature. The physics meta feature details the tangible, structural characteristics of a road, and the policy meta feature is fundamental for the operational and planning purposes of a road. These features provide strong support for constructing interpretable traffic forecasting and traffic causal analysis.

In Table 2, there are 6 famous existing datasets for **incident analysis**. Compared with them, our XTraffic includes multiple incident categories besides accidents. The category feature provides fundamental support for studying the impact of different incidents on traffic and also offers ground truth for detecting incidents beyond accidents. Also, XTraffic includes three kinds of traffic time series: traffic volume, road occupancy rate, and vehicle average speed. Such an integration significantly broadens the scope of analyzing post-incident impacts.

(2) **Comprehensive Road Meta Features in Multiple Aspects**. As shown in Table 4, XTraffic dataset includes a wide range of road meta-features, categorized into context, location, policy, and physics-related features. Context features include attributes like district and county, which help understand traffic patterns within different administrative or urban contexts. Location features provide precise spatial attributes such as road coordinates and segment information. Policy features cover regulatory aspects like speed limits, while physics features address road characteristics such as terrain type. This diverse set of meta-features allows for a holistic analysis of how various factors influence traffic behavior.

(3) **The Bridge between Traffic and Incidents**. XTraffic bridges the gap between traffic and incident data by integrating detailed traffic flow metrics (such as lane-level flow, speed, and occupancy) with comprehensive incident records (including various types of accidents). **From Traffic View**. As shown in Table 1, the existing datasets often lack incident data and have insufficient road-level granularity to effectively study the impact of incidents on traffic. For example, the effect of a traffic incident on one side of the road might be significantly different from the impact on the other side. XTraffic offers lane-level traffic flow, speed, and occupancy data with incident features, allowing for detailed analysis of traffic patterns under incident impact at a micro level. Also, the high resolution supports the identification of specific traffic bottlenecks, congestion patterns, and variations in traffic behavior that aggregate or road-level datasets might obscure. Researchers can perform fine-grained analysis to understand traffic dynamics under different incident impacts with greater precision. **From Incident View**. Compared to the existing opensource incidents dataset, as shown in Table 2, XTraffic has two advantages: (a)Not like other datasets only include accident type incidents, XTraffic covers 7 specific incident types, such as hazzards and road closures. (b)XTraffic includes three traffic time series (flow, speed, occupancy) more than other public datasets, even more than some non-public datasets (Lin & Li, 2020; Zhu et al., 2021). This allows for sophisticated analyses of how various incidents impact traffic conditions across different regions and times. Researchers can study patterns like the frequency and severity of incidents, their spatial distribution, and their temporal effects on traffic flow, providing a nuanced understanding of incident impacts that single-dataset approaches might miss. By combining incident data with detailed traffic metrics, our dataset facilitates advanced causal analysis, enabling researchers to determine how specific incidents influence traffic behavior over time. This capability supports the development of more effective traffic management strategies and predictive models that account for the immediate and long-term effects of incidents on traffic conditions.

3.2 Collection and Construction

Both incident and traffic data are collected from Caltrans Performance Measurement System (PEMS). We started our collection on April 20, 2024, and ended on May 10, 2024. The time span of the data covers the entire year of 2023. For **traffic data**, we removed the sensor with less than 50% observations of traffic volume and reserved the data of 16,972 sensors with meta-features. These sensors are located in 42 different cities and counties. We also collected comprehensive meta-features of these sensors. After excluding the features with the same value and features unrelated to traffic, 26 meta-features are reserved. These meta-features can be divided into 5 types as shown in Table 1. Full meta-features are in Table 6, Appx. A.3. As most methods in traffic forecasting are graph-based, the adjacency matrix is a key component for the model to learn spatial dependency. The construction of adjacency matrix is introduced in Appendix A.6.
For **incident data**, we removed repeated incident records and the records without absolute postmile (indicating the position and date-time). As the source and CA PM (we have Abs PM to locate the incident) are relatively redundant in the traffic analysis, thus also being removed. The reserved incident data includes 476,766 samples with 9 features. Identifying which nodes are impacted by an incident is crucial for leveraging incident records in traffic analysis. To facilitate this, we use a method that combines the freeway name and absolute postmile (Abs PM) markers to pinpoint sensors that might be affected by the incident. We provide two methods for this matching process: (1) involves matching only the nearest sensor on the same freeway as the incident, (2) involves setting a distance threshold and incorporating all sensors within this specified range.
Data imputation is also a crucial aspect of dataset application. However, Considering that different researchers may prefer different data cleaning methods (for example, to handle missing data, some may prefer

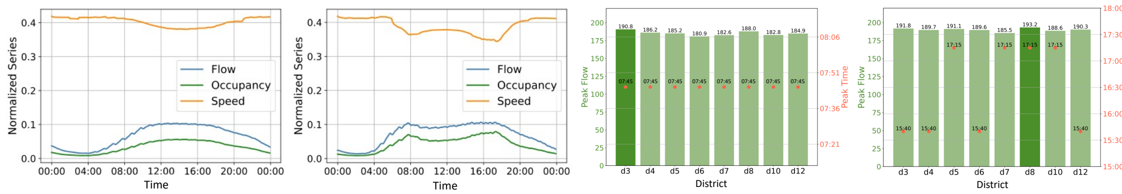

(a) Traffic time series variation on weekday (b) Traffic time series variation on weekend (c) Morning peak time and peak flow (d) Afternoon peak time and peak flow

Figure 2: (a) and (b) represent the average traffic variation of all sensors on weekdays and weekends, respectively. (c) and (d) represent the average peak flow and the peak time in different districts. The peak flow is calculated based on all sensors in the specific district. Deeper green indicates the highest peak flow.

zero filling for tasks such as classification, while some may avoid zero filling and prefer linear interpolation if the task is imputation so that they don't mix the ground-truth zero value and missing value). Thus, we believe providing the raw data we collected is better. In the experiments mentioned in Sections 4.2 and 4.3, we used zero-filling to address missing values in the traffic series features. More data imputation methods applications are discussed in Appendix A.5.

4 Experiments

4.1 Descriptive Analysis of XTraffic

To demonstrate the correlations between traffic conditions and incidents across various spatial and temporal dimensions, we conducted separate analyses for both traffic data and incident data.

4.1.1 Traffic Trending and Peak Hour Analysis

Traffic Time Series Variation Patterns. We defined weekdays as Monday through Friday and weekends as Saturday and Sunday. Within each group, we averaged traffic data from all sensors for the same time interval and normalized the data within each traffic category for visualization. As shown in Fig. 2(a) and (b), the results reveal a distinct evening peak in traffic between 4:00-5:00 PM on weekends. In contrast, weekdays exhibit both morning and evening peaks, with high traffic levels sustained throughout the day. Additionally, the statistical analysis shows an inverse relationship between speed and occupancy rate, as well as flow.

Traffic Peak Hour Analysis. We define the morning peak hour as between 6:00 and 10:00 and the evening peak hour as between 15:00 and 20:00. We calculated the average flow for each time interval across all sensors in different districts during peak hours and identified the peak flow values along with their corresponding peak times. As shown in Fig. 2(c) and (d), the peak times in the morning are consistent across districts, with similar traffic flow patterns. In the afternoon, however, two distinct peak times are observed: 15:40 and 17:15. Since our flow data is recorded by time intervals, 15:40 and 17:15 represent the time intervals 15:40-15:45 and 17:15-17:20, respectively.

4.1.2 Incidents Analysis on Hub and Fringe Nodes

At first, we summarize the distribution of incident durations and types. Fig. 2(a) reveals a long-tail distribution where most incidents are relatively short, but a few incidents last for an extended period. It also demonstrates the geographical distribution of incidents, with higher concentrations in urban areas. The pie chart in Fig. 3(b) shows hazards constitute the majority (52.2%). Next, we aim to further explore the frequency of incidents occurring on road segments under different levels of congestion. In the road network, each sensor can be considered as a node on a specific road. The hub node represents busy intersections and main roads, while the fringe node represents roads in remote areas or branch roads. Two cases for hub node and fringe node are shown in Fig. 3(c). Then, we conduct the following two analyses to reveal the relationship between different types of roads and incidents. (Details in Appendix A.7).

The Frequency of Different Types of Incidents Next to Hub and Fringe Nodes. We tally the total number of various types of incidents occurring next to hub nodes and fringe nodes. Fig. 3(d) shows that hazards and

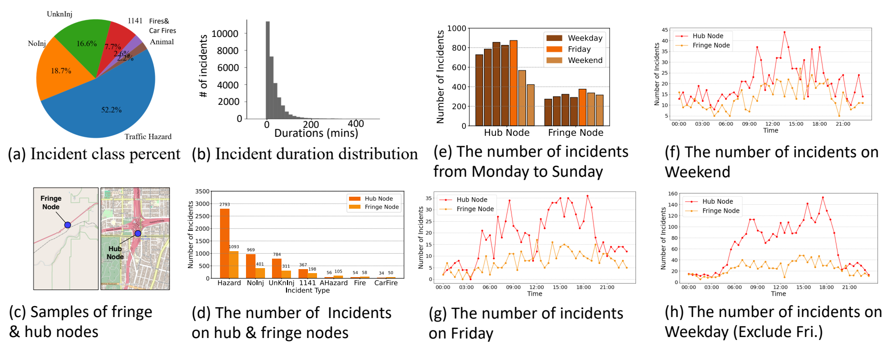

(a) Incident class percent (b) Incident duration distribution (e) The number of incidents from Monday to Sunday (f) The number of incidents on Weekend

(c) Samples of fringe & hub nodes (d) The number of Incidents on hub & fringe nodes (g) The number of incidents on Friday (h) The number of incidents on Weekday (Exclude Fri.)

Figure 3: Descriptive analysis of Incidents.(a) and (b) are calculated based on all incident records. (c)-(h) are calculated based on the incidents happening on hub/fringe nodes.

accidents are significantly more frequent on busy roads. In contrast, incidents related to fires and hazards caused by animals are more common on remote and less-traveled roads. This may be attributed to the higher activity of animals in less frequented areas and the increased risk of fire in remote areas due to reduced human attention. Based on the observations above, we find that the incident patterns for hub nodes and fringe nodes differ significantly. We are now curious about whether there are also differences in incidents between these two types of nodes in terms of time.

Incident Temporal Patterns on Hub and Fringe Nodes. Firstly, we analyze the distribution of incidents for two types of nodes throughout the week. Without considering incident types, we aggregated incidents by the day of the week. As shown in Fig. 3(e), there is a significant difference between hub nodes and fringe nodes. For **hub nodes**, the proportion of incidents on weekdays is higher than on weekends. This is expected, as downtown areas experience greater traffic volumes and are more prone to accidents on weekdays due to the high traffic flow in main roads and densely populated areas. On weekends, many people move to rural areas, reducing traffic pressure and leading to fewer incidents. In contrast, for **fringe nodes**, we can observe a reversed trend: there is a slight increase in the number of incidents on weekends compared to weekdays: this might be because the residents are moving back to rural areas for the weekends, thus bringing higher possibility of incidents. Interestingly, both types of nodes experience a peak in incidents on Fridays. Such a "Friday mood" will universally increase the incident risk regardless hub nodes or fringe nodes. Moreover, we conducted further analysis on the 30-minute variation of incidents. To analyze the differences in incident patterns between weekdays, Fridays (the day with the highest number of incidents), and weekends, we examined the variation in incident numbers throughout the day for both hub nodes and fringe nodes. The results, shown in Fig. 3(f), (g), and (h), reveal that the number of incidents on hub nodes and fringe nodes varies significantly on weekdays. Incidents typically occur during morning and evening peak hours. Compared to other weekdays, incidents on Fridays show greater fluctuations, likely due to Friday being a transitional day between weekdays and weekends.

4.2 Traffic Forecasting after Incidents

The existing models are effective in general traffic forecasting tasks. However, their performance under irregular volumes caused by incidents has not been thoroughly discussed. To assess these models' response in such conditions, we conduct irregular traffic forecasting based on XTraffic.

Experiment Setting: We selected prediction samples from the test set that one incident occurred within a 5-minute window. Due to the large volume of data, we chose to conduct experiments using traffic volume data from the San Bernardino (561 mainline sensors) within the XTraffic dataset for the first 3 months. All of the baselines are state-of-the-art in the spatial-temporal forecasting or traffic forecasting domain. Our forecasting experiments were implemented within the same software framework employed by (Liu et al., 2024).

Table 4: Performance among the SOTA time series classification methods across the datasets, with the top 1 in grey, 2nd in boldface, and 3rd underlined.

Methods	speed channel-only			occupancy channel-only			flow channel-only			All channels Mixed		
	Acc	Precision	Recall	Acc	Precision	Recall	Acc	Precision	Recall	Acc	Precision	Recall
DT	41.6%	41.5%	41.5%	**40.4%**	**40.2%**	**40.2%**	**39.4%**	**39.3%**	**39.3%**	**41.6%**	**41.4%**	**41.5%**
TS2Vec	36.6%	36.2%	36.2%	36.6%	36.5%	36.4%	37.3%	37.0%	37.0%	37.3%	37.0%	37.0%
gMLP	**41.3%**	**41.2%**	**41.1%**	38.4%	38.3%	38.3%	37.3%	37.2%	37.2%	41.6%	41.5%	41.5%
Sequencer	35.8%	35.8%	35.6%	35.6%	35.3%	35.2%	34.1%	33.9%	33.9%	40.3%	40.2%	40.2%
OmniScaleCNN	35.7%	35.1%	35.1%	36.9%	36.3%	36.3%	37.0%	36.8%	36.8%	40.9%	40.8%	40.8%
PatchTST	38.3%	38.1%	38.1%	39.0%	38.6%	38.7%	39.5%	39.3%	39.3%	39.4%	39.4%	39.3%
FormerTime	35.9%	31.0%	33.4%	41.0%	41.1%	40.8%	37.8%	38.2%	37.3%	40.5%	40.5%	40.1%

Results. As shown in Table 3, **all baselines perform significantly better in predicting on the general test dataset compared to the incident test dataset**, since incidents added irregularity into the traffic systems. This suggests that investigating how to improve the performance of forecasting models on time series prediction following an incident is worthwhile and warrants further research and discussion. More details in Appx. A.8.

Table 3: The results in different horizons in Monterey (D5 Area). 'General' shows the performance of the model across all samples in the test set, while 'Incident' is on samples after an incident has occurred, with the top 1 in grey, 2nd in boldface, and 3rd underlined.

Test	**Model**	5 Mins (t=1)			15 Mins (t=3)			30 Mins (t=6)		
		MAE	MAPE	RMSE	MAE	MAPE	RMSE	MAE	MAPE	RMSE
General	LSTM	12.58	11.81	21.45	15.41	14.21	26.29	18.68	18.03	31.54
	ASTGCN	12.45	13.11	20.90	14.59	13.66	23.10	16.03	15.56	27.82
	DCRNN	11.90	**11.82**	**20.47**	13.41	**12.92**	**23.79**	**14.84**	14.32	**26.74**
	AGCRN	12.54	12.56	22.65	13.55	13.18	25.27	14.62	**14.24**	27.92
	GWNET	**11.99**	11.85	20.30	13.53	12.87	23.44	14.88	14.15	26.05
	STGODE	12.75	13.26	21.66	14.12	14.57	24.64	15.50	16.34	27.43
	DSTAGNN	13.18	12.15	21.93	16.37	18.82	27.41	19.99	19.97	33.73
	D^2STGNN	12.18	12.00	21.30	**13.48**	13.20	24.30	14.90	14.27	27.28
Incident	LSTM	14.17	10.13	23.75	17.41	15.38	29.43	20.93	14.33	34.05
	ASTGCN	14.06	10.55	23.22	16.42	15.06	27.63	18.40	12.59	30.48
	DCRNN	13.62	9.86	**23.04**	15.36	**14.35**	26.73	16.92	11.69	**29.38**
	AGCRN	14.48	10.98	25.41	15.96	14.78	28.78	17.21	11.78	31.42
	GWNET	**13.73**	10.44	22.90	15.60	14.50	26.73	**17.15**	**11.49**	29.07
	STGODE	14.50	10.71	24.49	16.20	15.19	27.69	17.55	12.29	30.17
	DSTAGNN	14.79	10.57	24.22	18.24	17.91	30.48	21.95	15.38	35.67
	D^2STGNN	**13.73**	**10.05**	23.30	**15.51**	14.22	27.29	**17.03**	11.46	30.23

4.3 Incident Classification

Since traffic incidents typically affect the traffic on roads, it is viable to deduce the traffic conditions based on the dynamics of the parameters. In this work, a time series classification task is designed on XTraffic, which involves inferring incident categories based on the traffic during particular time slots detected by the sensors.

Experimental setting. Since traffic sensors are not always available at the site of an incident, we start by identifying the nearest sensor affected by each incident according to the distance (i.e., the ABS PM in Table 6). Then, we extract recorded indexes (traffic speed, lane occupancy, and traffic flow) in these sensors during a time window when the incident occurs. Augmented with normal data, these form the basis for characterizing traffic parameters, which fall into three categories: "accidents", "hazards", and "normal". According to Fig. 3(b), we standardize the duration length as the 95th percentile, i.e., 2 hours (w=24). The task is defined as a multivariate time series classification which uses three-channel time series to infer the situations of the traffic. We selected representative baselines from various families including statistical learning, contrastive learning, sequential models and Transformer-based models. More details of experiments in Appx. A.9.

Performance Evaluation. From Table 4: (1) **The best classification can achieve 41% accuracy, indicating classifying traffic conditions based on traffic indexes is feasible (better than random guess).** Among the datasets with different inputted features, *DT* and *PatchTST* always outperform the baselines. *gMLP* also shows strong performance, notably achieving top ranks in several categories and particularly excelling in the mixed channels. (2) **Variability across channels.** Different methods exhibit varying degrees of effectiveness depending on the channel used, e.g., *Sequencer* performing better with speed and worse with flow, and *OmniScaleCNN* opposite. Thus, selecting appropriate features can guarantee the model effectiveness.(3) **Integrating multiple features often leads to better classification.** However, the performance gain is method-dependent. *DT* and *gMLP* show improvement, while *TS2Vec* and *OmniScaleCNN* benefit less.

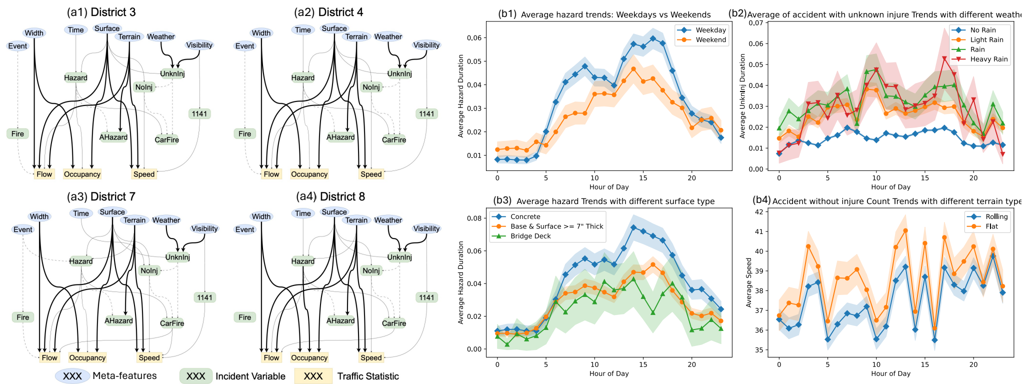

(a) Causal networks generated by MM-DAG. Thick solid arrows indicate strong causal relations, thin solid arrows for regular causal relations, and thin dashed arrows for weak relations.

(b) The average values and 95% confidence interval of outcome Y under different factor levels X in a causal relationship $X \rightarrow Y$, where $X \rightarrow Y$ can be: (b1) Time → Hazard; (b2) Weather → UnknInj; (b3) Surface → Hazard; (b4) Terrain → NoInj.

Figure 5: Global causal: (a) The learned DAG among meta-features, incidents, and traffic indexes. (b) The factual explanation for selected edges.

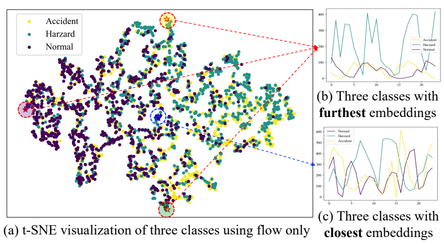

(a) t-SNE visualization of three classes using flow only

(b) Three classes with **furthest** embeddings

(c) Three classes with **closest** embeddings

Figure 4: Visualization of the representation of the time series on the dataset, extracted from the last hidden layer of *OmniScaleCNN*.

Fig. 4(a) visualizes the extracted feature from *OmniScaleCNN* by t-SNE (Van der Maaten & Hinton, 2008) using flow data.The selected furthest embeddings (in Fig. 4(b)) shows clear distinct flows between the three classes, yet the closest embeddings (Fig. 4(c)) not. (1) **There are distinct and separated patterns in the embeddings of traffic incidents located in corner and center areas**, which facilitates classification, causing better performance than random guess. (2) **Not all incidents impact traffic indices largely**. As car fires and accidents with no injuries are short-lived, these hard cases confuse the classifier since the traffic patterns do not change significantly.

4.4 Global Traffic Causal Analysis

Experiment Setting. In our XTraffic dataset, we have static variables, e.g., road information, represented as scalar and vector, and dynamic variables, e.g., accidents and traffic flow, represented as functional data. Considering the multimodal nature of the variables, we employ MM-DAG (Lan et al., 2023) to construct the causal network in different districts. We collect data on 17 variables across four districts with the highest incident rates throughout 2023. These variables fall into three categories: (1) meta-feature variables, e.g., temporal, environmental, road structural information; (2) incident variables, i.e., the occurrence of incidents; and (3) traffic statistics, which reflect traffic conditions. (Details in Table 7, Appx. A.10). We consider the data collected at each road node for each day as a single sample, using a granularity of one hour.

Results. Fig. 5(a) illustrates the four causal networks derived by MM-DAG. (1) **Certain static variables are essential**; such as road surface, terrain, and road width, they exert significant influences on the incidence of traffic events and the overall traffic conditions. (2) **The static variables' impacts are consistent**: Across various districts, due to their inherent properties, these underlying attributes consistently influence road and traffic dynamics across different regions. (3) **Dynamic variables like time, weather, and visibility also affect traffic incidents, though their causal relationships appear to be weaker and vary by district**. Like, causal links from events to fire and to hazards show variability and weaker connections in different districts. We further explain four significant edges. In Fig. 5(b1), the probability of encountering hazards is higher during the early morning (5 AM to 8 AM) and late afternoon (after 3 PM) on weekdays compared to weekends, likely due to increased traffic flow during peak commuting hours. In Fig. 5(b2), rain increases the probability of accidents compared to dry conditions, but the amount of rainfall does not significantly affect the accident rate. In Fig. 5(b3), bridges and road surfaces with a base thickness of >7 inches have a lower probability of hazards compared to concrete surfaces. This may be due to the enhanced durability and grip provided by thicker road surfaces and bridge constructions. In Fig. 5(b4), flat terrain is associated with higher average speeds compared to rolling terrains. The tendency for higher speeds on flat terrains is likely due to the reduced need for vehicles to decelerate for climbs or curves, allowing for more consistent and faster travel.

4.5 Local Causal Analysis for Road Relations

To demonstrate the value of our XTraffic dataset in revealing the causal relations among the roads, we conduct local causal analysis on a real case from XTraffic. We employ the PCMCI$^+$ (Runge, 2020) algorithm for causal structure learning. Since the underlying ground truth of causal dependencies is unknown, the hyperparameters, e.g., significance level and maximum time lag, are set for better interpretability.

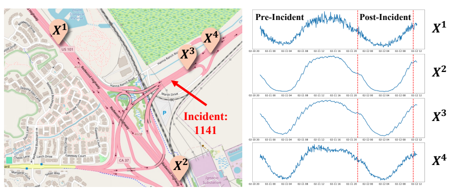

(a1) Road Network (a2) Traffic Flow Series

(a) Demonstration of Demonstration of the Selected Case. (a1) Road network with four selected traffic nodes, i.e., four sensors recording traffic flow data. An incident coded 1141 occurred very close to X^3. This incident indicates that a traffic collision has occurred and that there are potential injuries requiring a medical response. (a2) Traffic flow series of the selected nodes.

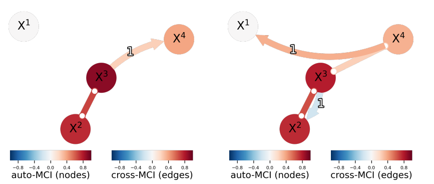

(b1) Pre-Incident Graph (b2) Post-Incident Graph

(b) Causal process graph learned by PCMCI$^+$. (b1) Pre-incident causal graph. (b2) Post-incident causal graph. Node and link colors depict the strength of auto-dependencies or cross-dependencies, respectively.

Figure 6: Case of Local Causal Analysis

Experiment Setting. In Fig. 6, we select the road network near an interchange in Novato, California. On the evening of February 11, 2023, a traffic incident "1141" occurred at the eastbound exit of the interchange. This incident indicates that a traffic collision occurred and that there were potential injuries requiring a medical response. We then select four traffic nodes, represented by their traffic flow indexes, $\{X^1, X^2, X^3, X^4\}$, that might be affected by the traffic incident. We see from Fig. 6 (a2) that the decrease in traffic flow of X^3, which is the node closest to the incident, significantly accelerated after the incident occurred.

Results. The causal graphs learned by PCMCI$^+$ are in Fig. 6 (b), where the colors depict the strength of causal dependencies and the label of a link represents the time lag of causal dependencies. The pre-incident causal structure matches the common understanding about traffic propagation, indicating that traffic flow propagates from X^2 through X^3 to X^4. Compared to the pre-incident graph, the post-incident graph has two additional lagged causal links $X^3 \xrightarrow{\text{lag } 1} X^2$ and $X^4 \xrightarrow{\text{lag } 1} X^1$. In such a complicated dynamic traffic system, explaining the change of causal dependencies is challenging and we endeavour to provide some conjectures for reference. Due to the traffic collision between X^2 and X^3, congestion likely occurred near X^3, reducing the traffic flow at each time slot. However, the traffic demand from X^2 to X^3 did not decrease in the short term, causing the congestion to gradually spread to X^2. The congestion at the eastbound exit of the interchange led to a decrease in traffic demand from X^1 to X^4. Fewer vehicles chose to slow down to enter the ramp, causing increased speed and higher traffic flow at X^1. (Details in Appx. A.11.)

5 Conclusion

We propose a pioneering traffic and incident dataset XTraffic. It integrates traffic flow data with incident records and road comprehensive meta-features, filling a significant gap in traffic analysis and Incident analysis. XTraffic lays a solid groundwork for research focused on understanding traffic dynamics, causality, and interrelationships. Through four groups of experiments, we demonstrate that our dataset offers expanded possibilities for research in traffic forecasting, incident classification, and detection, as well as causal analysis. Limitations and future work are discussed in Appendix A.12.

REFERENCES

Tariq Alsahfi. Spatial and temporal analysis of road traffic accidents in major californian cities using a geographic information system. *ISPRS International Journal of Geo-Information*, 13(5):157, 2024.

Ove Andersen and Kristian Torp. Dynamic spatio-temporal integration of traffic accident data. In *Proceedings of the 26th ACM SIGSPATIAL International Conference on Advances in Geographic Information Systems*, pp. 596–599, 2018.

Taif Anjum, Beiyu Lin, and Apurva Narayan. Leveraging spatio-temporal features to forecast time-to-accident. In *Proceedings of the 30th International Conference on Advances in Geographic Information Systems*, pp. 1–2, 2022.

Lei Bai, Lina Yao, Can Li, Xianzhi Wang, and Can Wang. Adaptive graph convolutional recurrent network for traffic forecasting. *Advances in neural information processing systems*, 33:17804–17815, 2020.

Tarikwa Tesfa Bedane. Road traffic accident dataset of addis ababa city. *Addis Ababa*, 2020.

Mingyue Cheng, Qi Liu, Zhiding Liu, Zhi Li, Yucong Luo, and Enhong Chen. Formertime: Hierarchical multi-scale representations for multivariate time series classification. In *Proceedings of the ACM Web Conference 2023*, pp. 1437–1445, 2023.

Jeongwhan Choi, Hwangyong Choi, Jeehyun Hwang, and Noseong Park. Graph neural controlled differential equations for traffic forecasting. In *Proceedings of the AAAI Conference on Artificial Intelligence*, volume 36, pp. 6367–6374, 2022.

Janez Demšar. Statistical comparisons of classifiers over multiple data sets. *The Journal of Machine learning research*, 7:1–30, 2006.

Chicago Police Department. Chicago traffic crashes, 2024. URL `https://data.cityofchicago.org/Transportation/Traffic-Crashes-Crashes/85ca-t3if/`.

New York City Police Department. New york city motor vehicle collisions, 2022. URL `https://data.cityofnewyork.us/Public-Safety/Motor-Vehicle-CollisionsCrashes/h9gi-nx95`.

Zheng Fang, Qingqing Long, Guojie Song, and Kunqing Xie. Spatial-temporal graph ode networks for traffic flow forecasting. In *Proceedings of the 27th ACM SIGKDD Conference on Knowledge Discovery & Data Mining*, pp. 364–373, 2021.

J Golze, U Feuerhake, C Koetsier, and M Sester. Impact analysis of accidents on the traffic flow based on massive floating car data. *The International Archives of the Photogrammetry, Remote Sensing and Spatial Information Sciences; XLIII-B4-2021*, 43:95–102, 2021.

Shengnan Guo, Youfang Lin, Ning Feng, Chao Song, and Huaiyu Wan. Attention based spatial-temporal graph convolutional networks for traffic flow forecasting. In *Proceedings of the AAAI Conference on Artificial Intelligence*, volume 33, pp. 922–929, 2019.

Zhengang Guo, Yingfeng Zhang, Jingxiang Lv, Yang Liu, and Ying Liu. An online learning collaborative method for traffic forecasting and routing optimization. *IEEE Transactions on Intelligent Transportation Systems*, 22(10):6634–6645, 2021. doi: 10.1109/TITS.2020.2986158.

Sepp Hochreiter and Jürgen Schmidhuber. Long short-term memory. *Neural computation*, 9(8):1735–1780, 1997.

Yayao Hong, Hang Zhu, Tieqi Shou, Zeyu Wang, Liyue Chen, Leye Wang, Cheng Wang, and Longbiao Chen. Storm: A spatio-temporal context-aware model for predicting event-triggered abnormal crowd traffic. *IEEE Transactions on Intelligent Transportation Systems*, 2024.

Baixiang Huang, Bryan Hooi, and Kai Shu. Tap: A comprehensive data repository for traffic accident prediction in road networks. In *Proceedings of the 31st ACM International Conference on Advances in Geographic Information Systems*, pp. 1–4, 2023.

Weiwei Jiang and Jiayun Luo. Graph neural network for traffic forecasting: A survey. *Expert Systems with Applications*, pp. 117921, 2022.

Shiyong Lan, Yitong Ma, Weikang Huang, Wenwu Wang, Hongyu Yang, and Pyang Li. Dstagnn: Dynamic spatial-temporal aware graph neural network for traffic flow forecasting. In *International Conference on Machine Learning*, pp. 11906–11917. PMLR, 2022.

Tian Lan, Ziyue Li, Zhishuai Li, Lei Bai, Man Li, Fugee Tsung, Wolfgang Ketter, Rui Zhao, and Chen Zhang. Mm-dag: Multi-task dag learning for multi-modal data-with application for traffic congestion analysis. In *Proceedings of the 29th ACM SIGKDD Conference on Knowledge Discovery and Data Mining*, pp. 1188–1199, 2023.

Tian Lan, Ziyue Li, Junpeng Lin, Zhishuai Li, Lei Bai, Man Li, Fugee Tsung, Rui Zhao, and Chen Zhang. Multifun-dag: Multivariate functional directed acyclic graph. *arXiv preprint arXiv:2404.13836*, 2024.

Dapeng Li, Joerg Sander, Mario A Nascimento, and Dae-Won Kwon. Discovering spatial co-clustering patterns in traffic collision data. In *Proceedings of the Sixth ACM SIGSPATIAL International Workshop on Computational Transportation Science*, pp. 55–60, 2013.

Guanyao Li, Shuhan Zhong, Xingdong Deng, Letian Xiang, S-H Gary Chan, Ruiyuan Li, Yang Liu, Ming Zhang, Chih-Chieh Hung, and Wen-Chih Peng. A lightweight and accurate spatial-temporal transformer for traffic forecasting. *IEEE Transactions on Knowledge and Data Engineering*, 2022.

Ruimin Li, Francisco C Pereira, and Moshe E Ben-Akiva. Overview of traffic incident duration analysis and prediction. *European transport research review*, 10(2):1–13, 2018a.

Yaguang Li, Rose Yu, Cyrus Shahabi, and Yan Liu. Diffusion convolutional recurrent neural network: Data-driven traffic forecasting. In *International Conference on Learning Representations (ICLR)*, 2018b.

Junpeng Lin, Ziyue Li, Zhishuai Li, Lei Bai, Rui Zhao, and Chen Zhang. Dynamic causal graph convolutional network for traffic prediction. In *2023 IEEE 19th International Conference on Automation Science and Engineering (CASE)*, pp. 1–8. IEEE, 2023.

Yunduan Lin and Ruimin Li. Real-time traffic accidents post-impact prediction: Based on crowdsourcing data. *Accident Analysis & Prevention*, 145:105696, 2020.

Dachuan Liu, Jin Wang, Shuo Shang, and Peng Han. Msdr: Multi-step dependency relation networks for spatial temporal forecasting. In *Proceedings of the 28th ACM SIGKDD Conference on Knowledge Discovery and Data Mining*, pp. 1042–1050, 2022a.

Hanxiao Liu, Zihang Dai, David So, and Quoc V Le. Pay attention to mlps. *Advances in neural information processing systems*, 34:9204–9215, 2021.

Xu Liu, Yutong Xia, Yuxuan Liang, Junfeng Hu, Yiwei Wang, Lei Bai, Chao Huang, Zhenguang Liu, Bryan Hooi, and Roger Zimmermann. Largest: A benchmark dataset for large-scale traffic forecasting. *Advances in Neural Information Processing Systems*, 36, 2024.

Zichuan Liu, Rui Zhang, Chen Wang, Zhu Xiao, and Hongbo Jiang. Spatial-temporal conv-sequence learning with accident encoding for traffic flow prediction. *IEEE Transactions on Network Science and Engineering*, 9(3):1765–1775, 2022b.

Sen Luan, Ruimin Ke, Zhou Huang, and Xiaolei Ma. Traffic congestion propagation inference using dynamic bayesian graph convolution network. *Transportation research part C: emerging technologies*, 135:103526, 2022.

Dennis Luxen and Christian Vetter. Real-time routing with openstreetmap data. In *Proceedings of the 19th ACM SIGSPATIAL international conference on advances in geographic information systems*, pp. 513–516, 2011.

Sobhan Moosavi, Mohammad Hossein Samavatian, Srinivasan Parthasarathy, Radu Teodorescu, and Rajiv Ramnath. Accident risk prediction based on heterogeneous sparse data: New dataset and insights. In *Proceedings of the 27th ACM SIGSPATIAL international conference on advances in geographic information systems*, pp. 33–42, 2019.

Yuqi Nie, Nam H Nguyen, Phanwadee Sinthong, and Jayant Kalagnanam. A time series is worth 64 words: Long-term forecasting with transformers. In *The Eleventh International Conference on Learning Representations*, 2022.

New York State Department of Motor Vehicles. New york state motor vehicle crashes, 2023. URL `https://data.ny.gov/Transportation/Motor-Vehicle-Crashes-VehicleInformation-Three-Ye/xe9x-a24f`.

UK Department of Transport. Uk accidents, 2016. URL `https://www.kaggle.com/datasets/daveianhickey/2000-16-traffic-flow-england-scotland-wales`.

Roxana Pamfil, Nisara Sriwattanaworachai, Shaan Desai, Philip Pilgerstorfer, Konstantinos Georgatzis, Paul Beaumont, and Bryon Aragam. Dynotears: Structure learning from time-series data. In *International Conference on Artificial Intelligence and Statistics*, pp. 1595–1605. Pmlr, 2020.

Nipun Ramakrishnan and Tarun Soni. Network traffic prediction using recurrent neural networks. In *2018 17th IEEE International Conference on Machine Learning and Applications (ICMLA)*, pp. 187–193. IEEE, 2018.

Jakob Runge. Discovering contemporaneous and lagged causal relations in autocorrelated nonlinear time series datasets. In *Conference on Uncertainty in Artificial Intelligence*, pp. 1388–1397. Pmlr, 2020.

Zezhi Shao, Zhao Zhang, Wei Wei, Fei Wang, Yongjun Xu, Xin Cao, and Christian S. Jensen. Decoupled dynamic spatial-temporal graph neural network for traffic forecasting. *Proc. VLDB Endow.*, 15(11): 2733–2746, sep 2022. ISSN 2150-8097.

Yunzhi Shi, Raj Biswas, Mehdi Noori, Michael Kilberry, John Oram, Joe Mays, Sachin Kharude, Dinesh Rao, and Xin Chen. Predicting road accident risk using geospatial data and machine learning (demo paper). In *Proceedings of the 29th International Conference on Advances in Geographic Information Systems*, pp. 512–515, 2021.

Chao Song, Youfang Lin, Shengnan Guo, and Huaiyu Wan. Spatial-temporal synchronous graph convolutional networks: A new framework for spatial-temporal network data forecasting. In *Proceedings of the AAAI Conference on Artificial Intelligence*, volume 34, pp. 914–921, 2020.

Cheng Tan, Siyuan Li, Zhangyang Gao, Wenfei Guan, Zedong Wang, Zicheng Liu, Lirong Wu, and Stan Z Li. Openstl: A comprehensive benchmark of spatio-temporal predictive learning. *Advances in Neural Information Processing Systems*, 36:69819–69831, 2023.

Wensi Tang, Guodong Long, Lu Liu, Tianyi Zhou, Michael Blumenstein, and Jing Jiang. Omni-scale cnns: a simple and effective kernel size configuration for time series classification. In *International Conference on Learning Representations*, 2021.

Yuki Tatsunami and Masato Taki. Sequencer: Deep lstm for image classification. *Advances in Neural Information Processing Systems*, 35:38204–38217, 2022.

Laurens Van der Maaten and Geoffrey Hinton. Visualizing data using t-sne. *Journal of machine learning research*, 9(11), 2008.

Z Wu, S Pan, G Long, J Jiang, and C Zhang. Graph wavenet for deep spatial-temporal graph modeling. In *The 28th International Joint Conference on Artificial Intelligence (IJCAI)*, 2019.

Zonghan Wu, Shirui Pan, Fengwen Chen, Guodong Long, Chengqi Zhang, and S Yu Philip. A comprehensive survey on graph neural networks. *IEEE transactions on neural networks and learning systems*, 32(1):4–24, 2020.

Qinge Xie, Tiancheng Guo, Yang Chen, Yu Xiao, Xin Wang, and Ben Y Zhao. Deep graph convolutional networks for incident-driven traffic speed prediction. In *Proceedings of the 29th ACM international conference on information & knowledge management*, pp. 1665–1674, 2020.

Sai Deepthi Yeddula, Chen Jiang, Bo Hui, and Wei-Shinn Ku. Traffic accident hotspot prediction using temporal convolutional networks: A spatio-temporal approach. In *Proceedings of the 31st ACM International Conference on Advances in Geographic Information Systems*, pp. 1–4, 2023.

Bing Yu, Haoteng Yin, and Zhanxing Zhu. Spatio-temporal graph convolutional networks: a deep learning framework for traffic forecasting. In *Proceedings of the 27th International Joint Conference on Artificial Intelligence*, pp. 3634–3640, 2018.

Haitao Yuan and Guoliang Li. A survey of traffic prediction: from spatio-temporal data to intelligent transportation. *Data Science and Engineering*, 6(1):63–85, 2021.

Zhihan Yue, Yujing Wang, Juanyong Duan, Tianmeng Yang, Congrui Huang, Yunhai Tong, and Bixiong Xu. Ts2vec: Towards universal representation of time series. In *Proceedings of the AAAI Conference on Artificial Intelligence*, volume 36, pp. 8980–8987, 2022.

Chuanpan Zheng, Xiaoliang Fan, Cheng Wang, and Jianzhong Qi. Gman: A graph multi-attention network for traffic prediction. In *Proceedings of the AAAI conference on artificial intelligence*, volume 34, pp. 1234–1241, 2020.

Xun Zheng, Bryon Aragam, Pradeep K Ravikumar, and Eric P Xing. Dags with no tears: Continuous optimization for structure learning. *Advances in Neural Information Processing Systems*, 31, 2018.

Weiwei Zhu, Jinglin Wu, Ting Fu, Junhua Wang, Jie Zhang, and Qiangqiang Shangguan. Dynamic prediction of traffic incident duration on urban expressways: A deep learning approach based on lstm and mlp. *Journal of intelligent and connected vehicles*, 4(2):80–91, 2021.

A APPENDIX

In this Appendix, we will introduce the data sheet of XTraffic, the statement of responsibility, more details of XTraffic data, related work of the 4 traffic tasks, and the experiment settings of the Post-Incident Traffic Forecasting, Incident Classification, Global Causal Analysis, and Local Causal Analysis.

A.1 DATA SHEET OF XTRAFFIC

In this section, we follow the datasheet format (**?**) to answer the critical questions to a standard dataset.

A.1.1 MOTIVATION

- **For what purpose was the dataset created?** The XTraffic is the most recent in terms of the collection period and contains the largest number of sensors, covering three distinct types of traffic volume. This ensures the timeliness of traffic research, providing a robust foundation for studies aiming to capture and explain traffic dynamics, causation, and interrelations. XTraffic serves as a rigid testing bed and empirical support to justify model effectiveness and interoperability in deep learning and the traffic community.
- **Who created the dataset?** The Machine Intelligence and kNowledge Engineering (MINE) lab.
- **Who funded the creation of the dataset?** The creation of the dataset and research reported in this paper was supported by funding from King Abdullah University of Science and Technology (KAUST).

A.1.2 COMPOSITION

- **What do the instances that comprise the dataset represent.** See the Section 3 Data Introduction.
- **How many instances are there in total?** For traffic time series data, the total number of instances is 105120 (Time Slots Number) $\times$ 16,972 (Sensor Number) $\times$ 3 (Feature Number). For incidents, the instances is 476,766.
- **Does the dataset contain all possible instances or is it a sample (not necessarily random) of instances from a larger set?** All possible instances excluding the sensors with a large number of missing values.
- **What data does each instance consist of?** See the Section 3 Data Introduction.
- **Is there a label or target associated with each instance?** See the Section 3 Data Introduction.
- **Is any information missing from individual instances?** Raw data missing.
- **Are relationships between individual instances made explicit** Yes, they are connected by time, location, and sensor ID.
- **Are there recommended data splits?** For Traffic forecasting, we recommend the ratio of 6:2:2 for training, valid, and test dataset. It is a common setting (Shao et al., 2022; Guo et al., 2019).
- **Are there any errors, sources of noise, or redundancies in the dataset?** Yes. The traffic time series are collected from sensors, and it may not count all of the passing vehicles.
- **Is the dataset self-contained, or does it link to or otherwise rely on external resources?** No.
- **Does the dataset contain data that might be considered confidential?** No.
- **Does the dataset contain data that, if viewed directly, might be offensive, insulting, threatening, or might otherwise cause anxiety?** No.

A.1.3 COLLECTION PROCESS

- **How was the data associated with each instance acquired?** The data is directly observable.
- **What mechanisms or procedures were used to collect the data (e.g., hardware apparatuses or sensors, manual human curation, software programs, software APIs)?** We use the PeMS data table corresponding URLs to collect the data.
- **If the dataset is a sample from a larger set, what was the sampling strategy (e.g., deterministic, probabilistic with specific sampling probabilities)?** Not fit.
- **Who was involved in the data collection process (e.g., students, crowdworkers, contractors) and how were they compensated (e.g.,how much were crowdworkers paid)?** No person is involved in the collection process.
- **Over what timeframe was the data collected?** The data was collected from April 20, 2024, to May 10, 2024. The dataset covers the entire year of 2023.
- **Were any ethical review processes conducted (e.g., by an institutional review board)?** No.

A.1.4 PREPROCESSING/CLEANING/LABELING

- **Was any preprocessing/cleaning/labeling of the data done (e.g., discretization or bucketing, tokenization, part-of-speech tagging, SIFT feature extraction, removal of instances, processing of missing values)?**Yes. We construct the adjacency matrix for sensors in the road network.
- **Was the "raw" data saved in addition to the preprocessed/cleaned/labeled data (e.g., to support unanticipated future uses)?** Yes.
- **Is the software that was used to preprocess/clean/label the data available?** The code is released in our GitHub repository `https://anonymous.4open.science/r/XTraffic-E069`

A.1.5 USES

- **Has the dataset been used for any tasks already?** No.
- **Is there a repository that links to any or all papers or systems that use the dataset?** No.
- **What (other) tasks could the dataset be used for?** Interpretable traffic forecasting, incident classification, incident duration prediction, and traffic causal analysis.
- **Is there anything about the composition of the dataset or the way it was collected and preprocessed/cleaned/labeled that might impact future uses?** The adjacency matrix is generated based on a threshold. It could be revised based on the task requirement.
- **Are there tasks for which the dataset should not be used?** No.

A.1.6 DISTRIBUTION

- **Will the dataset be distributed to third parties outside of the entity (e.g., company, institution, organization) on behalf of which the dataset was created?** Yes.
- **How will the dataset will be distributed (e.g., tarball on website, API, GitHub)?** Kaggle Dataset.
- **When will the dataset be distributed?** June 11, 2024.
- **Will the dataset be distributed under a copyright or other intellectual property (IP) license, and/or under applicable terms of use (ToU)?** Yes. Please see the section 4.
- **Have any third parties imposed IP-based or other restrictions on the data associated with the instances?** Yes. Please see the section 4.

- **Do any export controls or other regulatory restrictions apply to the dataset or to individual instances?** Yes. The use of data is required to satisfy the Caltrans Terms of Use of PeMS.

A.1.7 Maintenance

- **Who will be supporting/hosting/maintaining the dataset?** The first author of the dataset paper.
- **How can the owner/curator/manager of the dataset be contacted?** After accepting, we will release the email of the owner.
- **Is there an erratum?** No.
- **Will the dataset be updated?** Anual. If someone reports the error to us via GitHub, Kaggle or Email, we will check the data and fix the errors.
- **If the dataset relates to people, are there applicable limits on the retention of the data associated with the instances (e.g., were the individuals in question told that their data would be retained for a fixed period of time and then deleted)?** There is no person information included in XTraffic.
- **Will older versions of the dataset continue to be supported/hosted/maintained?** Yes. The largest difference between the old version and the new version is the time, and it's not hard to maintain the old versions. we will fix the errors reported.
- **If others want to extend/augment/build on/contribute to the dataset, is there a mechanism for them to do so?** No. We don't have enough resources to verify the external contributions.

A.2 Statement of Responsibility

According to the Ownership section in Caltrans Terms of Use of PeMS[1], we can collect and construct a dataset from the source and distribute it. We collected all of the data before 17/05/2024. More details and the introduction of the dataset can be found in the supplementary material. Our XTraffic is released under a CC BY-NC 4.0 International License[2]. The code for the experiments is released under an MIT License[3]. We claim that we are responsible for the data release and collection.

A.3 Details of XTraffic

Licence. According to the Ownership section in Caltrans Terms of Use of PEMS, we can collect and construct a dataset from the source and distribute it. We collected all of the data before 17/05/2024. More details and the introduction of the dataset are clarified in the Appendix A.3. Our XTraffic is released under a CC BY-NC 4.0 International License. The code for the experiments is released under a MIT License.

Meta data. The meta data for the XTraffic dataset can be accessed at the `https://anonymous.4open.science/r/XTraffic-E069/xtraffic-metadata.json`.

[1] https://pems.dot.ca.gov/?view=tou
[2] https://creativecommons.org/licenses/by-nc/4.0
[3] https://opensource.org/licenses/MIT

Incidents. The details of incident data features are shown in Table 5.

Table 5: Meta Feature Introduction

Feature	Type	Description
Incident ID	Integer	Unique identifier for each recorded traffic incident.
Duration	Integer	Length of the incident measured in minutes from start to resolution.
Abs PM	Float	Point of the incident in absolute postmile notation along the road.
Fwy	String	The freeway name where the incident occurred.
AREA	String	The city or town where the incident took place.
DESCRIPTION	String	A brief narrative describing the specifics of the incident.
LOCATION	String	The exact address on the freeway where the incident happened.
Type	String	Category of the incident, such as accident, hazard, or road closure.
dt	DateTime	Timestamp indicating when the incident was first reported.

Lane meta features. The details of the lane meta features are in Table 6,

Table 6: Meta Feature Introduction

Feature	Type	Description
Sensor ID	String	Unique identifier for each traffic sensor.
Inner Shoulder Width	Float	Width in meters of the inner shoulder on the lane.
Outer Shoulder Width	Float	Width in meters of the outer shoulder on the lane.
Functional Class	String	Classification of roads based on the function they provide.
Inner Median Type	String	Type of median on the inner side of the road.
Inner Median Width	Float	Width in meters of the median on the inner side of the road.
Road Width	Float	Total width in meters from one side to the other.
Lane Width	Float	Width in meters of each traffic lane on the road.
Design Speed Limit	Integer	Maximum speed limit designed for the road in kilometers per hour.
Terrain	String	Physical features and shape of a landscape, e.g., flat, mountainous.
Population	String	Type of terrain surrounding the road, e.g., urban, rural.
Barrier	String	Description of any barriers along the road, e.g., guardrail, none.
Surface	String	Road surface type, e.g., asphalt, concrete.
Roadway Use	String	Primary use of the road, e.g., commercial, residential.
Length	Integer	The total length of the lane on the road.
Latitude	Float	Geographical latitude of the road's location.
Longitude	Float	Geographical longitude of the road's location.
Abs PM	Float	Point of measurement in absolute postmile notation along the road.
Direction	String	The direction of the lane, e.g., East, North.
Fwy	String	The name of the freeway where the sensor is located in.
District	Integer	The district ID, e.g..
County	String	The county where the sensor is located in, e.g., Orange, Los Angeles.
City	String	The city where the sensor is located in, e.g., Marina, Oakland.
Sensor Type	String	The sensor cateogry, e.g., radars, magnetometers.
Type	String	The level of the road, e.g., mainline, On Ramp.
HOV	String	Whether it is HOV lane or not

A.4 PRELIMINARY OF FOUR INTENDED TASKS

Traffic Forecasting is to predict traffic indexes at nodes within a road network based on historical data collected by sensors at each node. Consider a traffic road network represented as a graph $G = (V, E)$, where V denotes the set of N traffic nodes, with $|V| = N$, and E represents the set of undirected edges. An edge $E_{ij} = 1$ indicates a physical connection between nodes i and j in the road network; otherwise, $E_{ij} = 0$. Traffic volume data is recorded by sensors in evenly spaced time intervals and can be represented as a sequence of matrices $(\mathbf{X}^1, \mathbf{X}^2, ..., \mathbf{X}^T) \in \mathbb{R}^{N\times T}$, where $\mathbf{X}^t$ is the matrix of volume signals $(x_1^t, x_2^t, ..., x_N^t)$ at time slot t for all N nodes.

The goal in traffic flow forecasting is to devise a function $\mathcal{F}_1$ that uses the observed traffic data from T_1 time slots to predict the traffic volumes for the subsequent T_2 time slots: $(\mathbf{X}^{t-T_1+1}, ..., \mathbf{X}^t) \xrightarrow{\mathcal{F}_1} (\hat{\mathbf{X}}^{t+1}, ..., \hat{\mathbf{X}}^{t+T_2})$, where $\hat{\mathbf{X}}^{t+1}$ represents the prediction at time $t+1$, and a general loss function is defined as: $\min \frac{1}{T_2}\sum_{i=1}^{T_2} \mathcal{L}_1(\hat{\mathbf{X}}^i, \mathbf{X}^i)$.

Incident Classification is to identify traffic incidents using traffic indexes. Since traffic sensors are not always available at the site of an incident, for brevity, we associate the parameters in the nearest single sensor to classify an incident, rather than aggregating data from multiple neighboring sensors. For the i-th paired sample ($\mathbf{X}_i$, y_i) in the dataset $\mathcal{D}$, $\mathbf{X}_i^c \in \mathbb{R}^{C\times w}$ is the input and y_i represents its corresponding label, where C denotes the number of multivariate feature channels (e.g., speed and flow) and w indicates the time window at the post-incident timing t. There is $\mathbf{X}_i^c = \{\mathbf{x}^t, \mathbf{x}^{t+1}, ..., \mathbf{x}^{t+w-1}\}$ and the j-th entity $\mathbf{x}^{t+j} \in \mathbb{R}^C$. The classification task is: $\hat{y}_i = \mathcal{F}_2(\mathbf{X}_i^c; \Theta)$, where $\hat{y}_i$ is the predicted result, $\mathcal{F}_2$ is the classifier, and Θ is trainable parameters. The overall objective is to minimize the classification loss $\mathcal{L}_2$ (e.g., cross-entropy) on $\mathcal{D}$: $\min_\Theta \frac{1}{|\mathcal{D}|}\sum_{i=1}^{|\mathcal{D}|} \mathcal{L}_2(\mathcal{F}_2(\mathbf{X}_i^c; \Theta), y_i)$.

Causal Analysis and Directed Acyclic Graph (DAG) In causal analysis, the primary objective is to elucidate the causal relationship, which is represented in a dynamic acyclic graph (DAG). Within a DAG, each node corresponds to a variable, and each directed edge delineates a causal relationship between two variables. The causal structural model enables the representation of a node's distribution w_i through $w_i = f_i(w_{pa_i}, e_i)$, where w_{pa_i} denotes the set of all parents of node w_i, and e_i represents the exogenous noise associated with node w_i. We consider two subtasks:
(1) ***Global Causal Analysis for The Whole System***. In global causal analysis, we focus on the problem that macro-level phenomena influence each other, such as the impact of weather on accident rates. Therefore, each node within the graph represents distinct variables like weather conditions, traffic accidents, or overall traffic statistics. This approach helps in understanding the broader implications of various environmental and systematic factors on traffic dynamics.
(2) ***Local Causal Analysis for Road Relations***. In local causal analysis, we focus on the temporal dependency structure underlying the complex traffic road network. We aim to find a graph $\mathcal{G}$ where the nodes are the variables representing traffic nodes at different lag-times and the links represent lagged or contemporaneous causal dependencies between traffic nodes. This approach helps in understanding how topologic of the road network affects traffic conditions.

A.5 DATA CLEANING

Besides filling zero and linear interpolation, there are also some specific filling models for traffic data. For example, ST-MVL[6] combined several empirical statistical models with user-based and item-based collaborative filtering to collectively fill in missing values in geo-sensory time series data. However, the model suffers from overlooking the global correlations of data. The [7] regards the raw data as a tensor and models the data recovery as a low-rank robust tensor completion via leveraging the inherent low-rank structure to address the issue. On the other hand, to discover the anomaly/dirty/outlier data, the [8] leverages DBSCAN to discover the outlier points in spatio-temporal data. Furthermore, it's necessary to repair the discovered dirty data. [9] proposes a metric to evaluate the dissimilarity between the raw dataset and the repaired one. Then it utilizes space- and time-distortion rules and employs a hybrid simulated-annealing approach to avoid local minima during the repair process. We will add the discussion of potential data cleaning methods in the final paper or on the dataset project website. Exploring better data-filling techniques to mitigate the impact of data gaps is an excellent direction for future research.

A.6 Construction of Adjacency Matrix

Typically, the adjacency matrix is constructed based on distance (Liu et al., 2024). In order to get the real travel distance, we set up an open-source rooting machine engine (Luxen & Vetter, 2011) based on OpenStreetMap, and calculate the shortest travel distance between two sensors based on the coordinate. One more precise adjacency matrix is constructed based on the direction of the lanes and the coordinates of two sensors A and B.

A.7 Definition of Hub and Fringe Nodes

We calculate the degree of each node using the adjacency matrix described in the paper. Nodes with the 500 highest degrees are classified as hub nodes, and those with the 500 lowest degrees are classified as fringe nodes. We match all incidents with the closest node/sensor and also remove the incident samples that the distance between the incident and its closest sensor is larger than 0.05 mile. We count the incident number of the hub nodes and fringe nodes, respectively.

A.8 Experiment Details on Post-Incident Traffic Forecasting

Baselines. The baselines we selected to do the forecasting experiments are typical models in traffic forecasting domain.

- **LSTM**(Hochreiter & Schmidhuber, 1997): A basic model focusing solely on the temporal relationships within traffic data.
- **ASTGCN**(Guo et al., 2019): Enhances the STGCN by incorporating an attention mechanism to better capture node correlations.
- **DCRNN**(Li et al., 2018b): An RNN-based model that utilizes diffusion convolution to model traffic flows.
- **AGCRN**(Bai et al., 2020): An adaptive model that combines RNN architecture with an attention mechanism to focus on spatial correlations.
- **GWNET**(Wu et al., 2019): Utilizes a gated mechanism in a TCN framework to filter out irrelevant information effectively.
- **STGODE**(Fang et al., 2021): Uses ordinary differential equations to dynamically model relationships among traffic nodes.
- **DSTAGNN**(Lan et al., 2022): Designed to dynamically capture changing correlations among traffic sensors.
- **D^{2}STGNN**(Shao et al., 2022): A dual-layer spatial-temporal GNN that addresses hidden correlations in traffic data for forecasting.

Implementation Details. We adhered to the identical experimental settings outlined within the work. We divided all the data into training, validation, and test sets in a 6:2:2 ratio. We set the batch size as 24 for DSTAGNN and 64 for all of other models. The learning rate is set as 0.001. Other hyperparameters of models are set as the same as the original settings. Our baselines follow the optimal settings from their sources. For the batch size in the training set, we used different settings to ensure that the model converges as quickly as possible during training. The batch size settings are mentioned in Section 4.2. For **LSTM**, the hidden layer dimension is set as 64, the last linear layer dimension is set as 512. For **ASTGCN**, the dimension of the attention layer is as 64. For **DCRNN**, the number of RNN layers is set as 2, and the dimension for each RNN layer is 64. For **AGCRN**, the hidden dimension is set as 64 for all cells and the embedding dimension is set as 10. For **GWNET**, the dimension of input and output linear layer are set as 32 and 512, respectively. The dimension of hidden layers is set as 256. For **STGODE**, the regular hyperparameter α is set as 0.8. The thresholds σ and ϵ of spatial adjacency matrix (AM) are set to 10 and 0.5 respectively, and the threshold ϵ of the semantic AM is set to 0.6. For **DSTAGNN**, the attention dimension is set as 32, and the number of attention heads is set as 3. For **D^{2}STGNN**, the hidden dimension is set as 32.

A.9 Experiment Details on Incident Classification

Baselines. We adopt the following representative time series classification baselines.

- **Decision Tree (DT)**: We tailor the canonical decision tree algorithm for the task, recursively partitioning data based on feature values to create a tree-like model that makes classifications at its leaf nodes.
- **TS2Vec** (Yue et al., 2022): It is a universal framework for learning robust and flexible time series representations using hierarchical contrastive learning over augmented context views, making the classification by a linear classifier.
- **gMLP** (Liu et al., 2021): It is a simple network architecture based solely on MLPs with gating, which performs as well as Transformers in key language and vision applications.
- **Sequencer** (Tatsunami & Taki, 2022): It models long-range dependencies using LSTMs without self-attention layers, which enhances performance by reducing the sequence length and creating spatially meaningful receptive fields.
- **OmniScaleCNN** (Tang et al., 2021): It is a 1D-CNN architecture that utilizes a set of prime number-based kernel sizes to efficiently capture optimal receptive field sizes without scale tuning across diverse time series classification tasks.
- **PatchTST** (Nie et al., 2022): It incorporates patching of time series into subseries-level patches and channel-independence to improve long-term forecasting accuracy based on the Transformer backbone.
- **FormerTime** (Cheng et al., 2023): It employs a hierarchical Transformer-based architecture to learn multi-scale feature maps and introduces an efficient temporal reduction attention mechanism and a context-aware positional encoding generator for multivariate time series classification.

Implementation Details. We randomly sampled 9,000 examples to experiment, 3,000 samples per category. The data is divided into training and testing sets in a 7:3 split.

We set the hyperparameters based on the recommended values in the original method and adjust them around those values, taking the parameter values corresponding to the best results as the final result. Specifically, the hyperparameters for each method are as follows:

For the **Decision Tree**, the minimum number of samples required for a leaf node is set to 1, and for splitting an internal node, it is set to 2. In **TS2Vec**, the pretraining stage has an output dimension of 320 and a hidden dimension of 64. The model is trained for 100 epochs with a batch size of 16, and the linear layer is chosen as the downstream classification module with $1e^{-3}$ learning rate. For **FormerTime**, the model is configured with 3 stages, each having 2 layers with a hidden size of 64. The number of slices per stage is 4, 2, 2, with

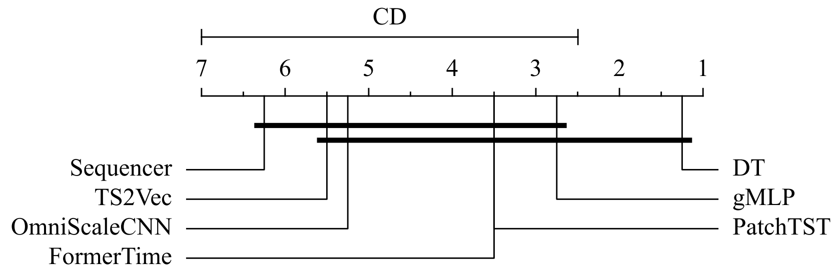

Figure 7: Critical difference diagram over the mean ranks of the compared methods

a stride of 4, 2, 2. The model is trained for 100 epochs with $1e^{-3}$ learning rate. In **PatchTST**, the patch length is set to 16, the stride to 8, the number of encoder layers to 2, the number of heads to 8, and the model dimension to 512. **gMLP** is configured with a patch size of 1, a model dimension of 256, a fully forward network dimension of 512, and a depth of 6. **PatchTST**, **TSSequencer**, **OmniScaleCNN**, and **gMLP** are trained for 100 epochs with a batch size of 128, and the learning rate of them is set as $3e^{-4}$.

More Results. Fig. 7 reports the critical difference diagram as presented in (Demšar, 2006), which compares the mean ranks of the baseline methods on the four datasets (three channel-only and all mixed) in the classification task. The thick horizontal lines in the diagram denote groups of methods whose performance differences are not statistically significant within the critical difference (CD) threshold. It can be seen that DT, gMLP, and PatchTST are among the top-performing methods with the lowest mean ranks, indicating their superior performance. Although DT, gMLP, and PatchTST are highlighted as top performers, the differences among the top five methods are not statistically significant since they are in a group, suggesting comparable effectiveness in this task.

A.10 Experiment Details on Global Causal Analysis

The introduction of MM-DAG. MM-DAG is a score-based causal discovery algorithm. It learns multiple DAGs with multimodal data where their consensus and consistency are maximized. For multimodal data, it proposes a multi-modal regression for linear causal relationship description of different variables by functional principal component analysis. For multitask learning, it uses causal difference to ensure the consistency. The overall optimization problem can be represented as:

$$
\begin{aligned}
\hat{\mathbf{C}}_{(1)}, ..., \hat{\mathbf{C}}_{(L)} = \underset{\mathbf{C}_{(1)},...,\mathbf{C}_{(L)}}{\arg\min} \sum_{l=1}^{L} \frac{1}{2N_l} \|\mathbf{A}_{(l)} - \mathbf{A}_{(l)}\mathbf{C}_{(l)}\|_F^2 \\
+ \rho \sum_{l_1,l_2} s_{l_1,l_2} DCD(\mathbf{W}_{(l_1)}, \mathbf{W}_{(l_2)}) + \lambda \sum_{l=1}^{L} \|\mathbf{C}_{(l)}\|_1 \\
\text{s.t. } h(\mathbf{W}_{(l)}) = \mathrm{tr}(e^{\mathbf{W}_{(l)}}) - P_l = 0, \forall l
\end{aligned}
$$

where $\mathbf{A}$ is variables after FPCA, $\mathbf{C}$ are causal matrix and $\mathbf{W}_{(l)ij} = \|\mathbf{C}_{(l)ij}\|_F^2$. s_{l_1,l_2} is the given constant reflecting the similarity between tasks l_1 and l_2, ρ controls the penalty of the difference in causal orders, where larger ρ means less tolerance of difference. λ controls the L_1-norm penalty of causal matrix which guarantees that edges are sparse. In our setting, we set $\lambda = 0.001$, $\rho = 1$ and $s_{l_1,l_2} = 1, \forall l_1, l_2$.

Explaination of the nodes: The details of the nodes in the global causal graph in listed in Table 7.

Constraints of the experiment:In learning DAG, two constraints are placed: (1) edges are not allowed to point toward meta-feature variables since meta-feature variables generally describe environmental and infrastructural contexts that inherently influence other variables rather than being influenced by them. (2) traffic statistics variables are restricted from directing edges towards other nodes since these statistics fundamentally represent outcomes or states of the traffic system, typically influenced by both high-level environmental conditions and specific incidents, rather than serving as direct causes themselves.

Table 7: The description and types of the variables used in traffic causal analysis

Category	Name	Type	Description
high-level variables	Time	Scalar	Day type indicator: $= 1$ if the day is a weekend; $= 0$ otherwise.
	Event	Scalar	Public holiday indicator: $= 1$ if the day is a public holiday; $= 0$ otherwise.
	Visibility	Functional	An integer ranged from 0 to 16 to indicate the visibility of the road in the district.
	Surface	Vector	Attributes describing road material, e.g., concrete, bridge deck.
	Terrain	Vector	Characteristics of the terrain surrounding the road, e.g., flat, rolling.
	Width	Scalar	The width of the road.
	Weather	Functional	An integer ranged from 0 (No rain) to 3 (Heavy rain).
incident variables	Hazard	Functional	Details of any hazards present, e.g., obstacles, spillage.
	NoInj	Functional	Records of accidents with no injuries.
	UnknInj	Functional	Records of accidents with unknown injury statuses.
	1141	Functional	Records of accidents needing an emergency response (coded 1141).
	Fire	Functional	Incidents involving vehicle fires or roadside fires.
	AHazard	Functional	Presence of animals on the road that could cause hazards.
	CarFire	Functional	Specific incidents involving car fires.
traffic statistics	Flow	Functional	Measures of traffic flow, typically in vehicles per hour.
	Occupancy	Functional	Percentage of the road occupied by vehicles at a given time.
	Speed	Functional	Average speed of traffic flow.

A.11 Experiment Details on Local Causal Analysis

In local causal analysis, We employ the PCMCI$^+$ algorithm to discover the causal relations in traffic data, which utilizes momentary conditional independence (MCI) test to determine the existence of causal links. Typically, the lagged and contemporaneous causal relations are displayed in a dynamic Bayesian network (DBN) as shown in Fig. 8 (a). In this work, to simplify the visualization, we choose to use the process graph as shown in Fig. 8 (b) to aggregate the information in the DBN. In both DBN and process graph, the link color denotes the magnitude of the causal effect measured by the MCI test statistic (e.g., the partial correlation coefficient). The label of a link lists all significant lags of cross-dependencies in process graph. Since we are more interested in the causal links between different traffic nodes, the links denoting auto-dependencies in DBN are summarized into node colors in process graph and the auto-dependency lags are omitted.

The choice of causal structure learning method influences the results of local causal analysis. Ideally, we would like to perform analysis on real cases or datasets with known underlying ground truth of causal dependencies. However, such cases or datasets are rare especially in complex dynamic scenarios such as traffic. To enhance the credibility of the learned causal structure, we use different causal discovery methods and verify the consistency of the results obtained by the different methods. Fig. 9 shows the pre-incident causal graphs of case I learned by score-based method DyNotears (Pamfil et al., 2020) and constrained-based method PCMCI$^+$ (Runge, 2020). The graph structures learned by both methods are similar, but the time lag of the link $X^3 \rightarrow X^4$ is different, which is greatly influenced by the sampling frequency of traffic data. Due to the limited number of samples affected by the incidents, we use PCMCI$^+$ to discover post-incident causal structure for its robustness with small sample size and high dimensionality.

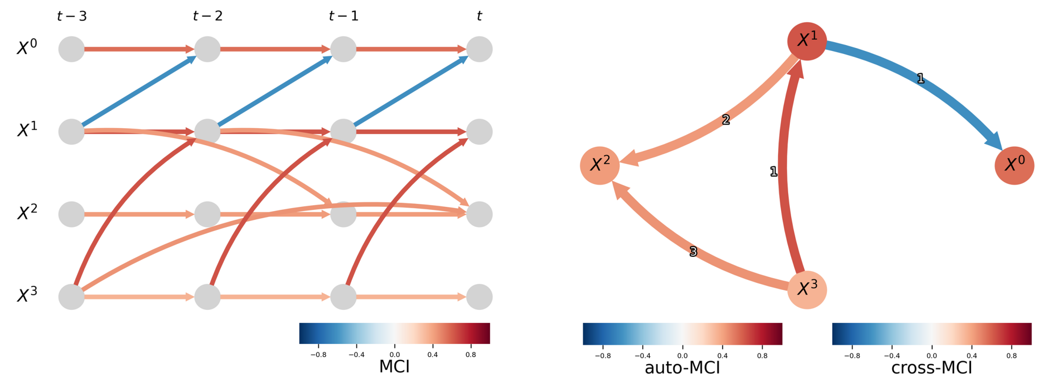

(a) Dynamic Bayesian Network **(b) Process Graph**

Figure 8: Examples of causal graphs for time series variables. (a) Dynamic Bayesian network (DBN). (b) Process graph which summarizes the information in DBN. Process graph aggregates the information in the DBN to simplify the causal structure visualization. While the process graph is nicer to look at, the time series graph better represents the spatio-temporal dependency structure from which causal pathways can be read off. In both graphs, link colors depict the magnitude of the cross-node causal effects as measured by the MCI test statistics. In process graph, node colors depict auto-dependency strength.

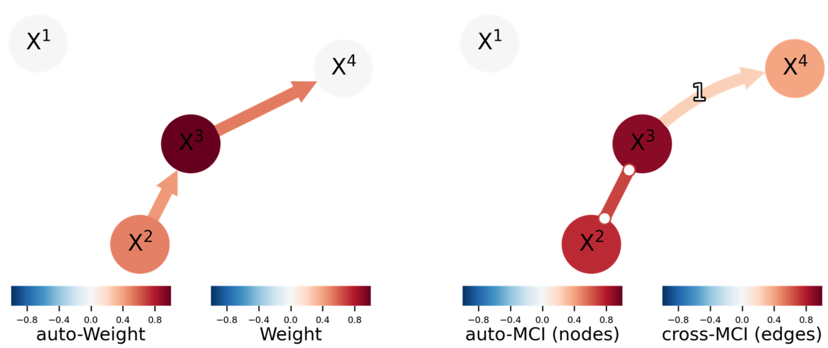

(a) DyNotears (Pre-incident) **(b) PCMCI+ (Pre-incident)**

Figure 9: Pre-Incident Causal Graphs for Local Causal Analysis Case Learned by Different Methods. (a) Process Graph Learned by DyNotears. (b) Process Graph Learned by PCMCI$^+$.

The primary Hyperparameters of $PCMCI^{+}$ are the maximum time delay τ_{max} and the significance threshold for the MCI test α_{PC}. The maximum time delay should be determined based on the specific application, reflecting the maximum expected causal time lag in the scenario under investigation. To identify this maximum time lag, we plot the results of the bivariate lagged conditional independence test. The significance threshold α_{PC} is adjusted on a case-by-case basis to ensure the derived causal structure is reasonable for the analysis. Further details about $PCMCI^{+}$ implementation and parameter tuning can be found in the public causal discovery tutorials [4]

A.12 Limitations and Future Work

Our dataset currently faces three limitations. (1) Although we integrate weather features into XTraffic, the weather data are not available to release. Our dataset lacks public well-integrated weather information for use. (2) Lack of incident precisely location. As shown in Fig. 6(a), The incident precisely latitude and longitude could be calculated based on the abs PM and the closest sensor location. We will release the location of incidents in the second version of XTraffic. (3) XTraffic is insufficient for cross-year seasonal analysis. We are currently collecting and organizing data from additional years. Based on the comprehensive January data we have gathered over multiple years, we conducted analyses, and the results are presented in Appendix A.13.

A.13 Extend Multi-Year Data Analysis

Currently, we have collected data for January 2021 and 2022 and we conducted two statistical analyses and two case studies.

We analyze the weekday and weekend daily trending variation in January based on all sensors excluding those not deployed sensors in 2021. Also, we compared the average flow on the hub road and fringe road during weekdays and weekends.

Year-on-Year Trending on Weekday and Weekday in January. Through year-on-year change analysis and observation, we identified unusual variations in traffic across different years. Due to data limitations, we conducted the analysis only for January data. We divided January traffic data from all sensors into two groups: weekdays and weekends. We then calculated the average traffic for each group, resulting in two distinct traffic change trends. To enhance visualization, we normalized the data by using three types of traffic as baselines and dividing the data from other years by these baselines. The analysis results are illustrated in Fig. 10(a) and (b).

In comparison to 2021, traffic flow increased in 2022, while the average speed decreased in line with the rise in traffic flow. However, in 2023, despite a decrease in traffic flow, traffic speed also declined, which may be attributed to the significant natural disasters in California that persisted until mid-January 2023.

Case Study on Hub Road and Fringe Road. To further explore traffic patterns, we selected a sensor located on a high-traffic segment to observe its daily traffic flow variations. We used the adjacency matrix described in Section 3.2 to compute the degree of each sensor and chose from the top 500 sensors with the highest degrees and no missing data for this analysis. We selected the sensor 717123 as shown in Fig. 11. Similar to the previous analysis, we categorized the traffic flow data from this sensor into weekday and weekend groups. Within each group, we averaged the data across three years. The results, illustrated in Fig. 12, reveal that for weekdays, 2023 still exhibited peak-hour trends. However, for weekends, there is a noticeable decline in traffic flow in 2023 compared to the other two years. This suggests that even under adverse weather conditions, a significant number of people continued to travel to their workplaces.

[4] https://github.com/jakobrunge/tigramite/blob/master/tutorials/causal_discovery/

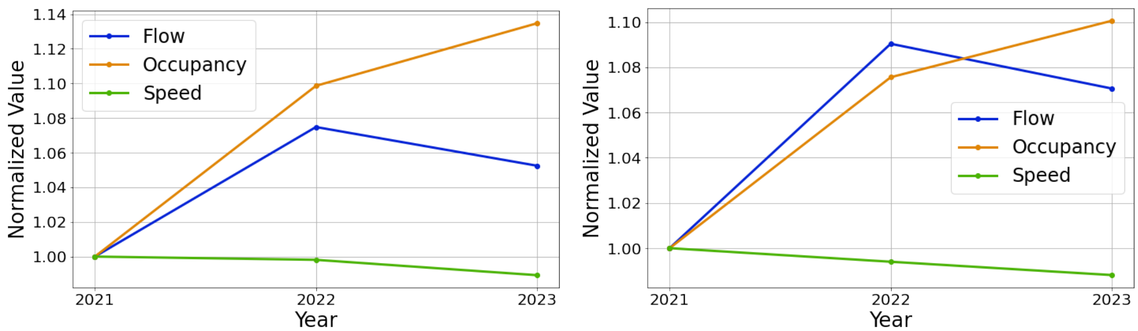

(a) Normalized Traffic on Weekday (b) Normalized Traffic on Weekend

Figure 10: (a) and (b) show the year-on-year change trending on Weekday and Weekend, respectively. The time series is normalized for visualization. In 2023, California suffered a long-term natural hazard including blood and storms. Although the traffic flow goes down, the occupancy increases.

Figure 11: The location of the selected sensor for the case study. the sensor without missing traffic flow data and with the largest 500 degree among 16,145 sensors.

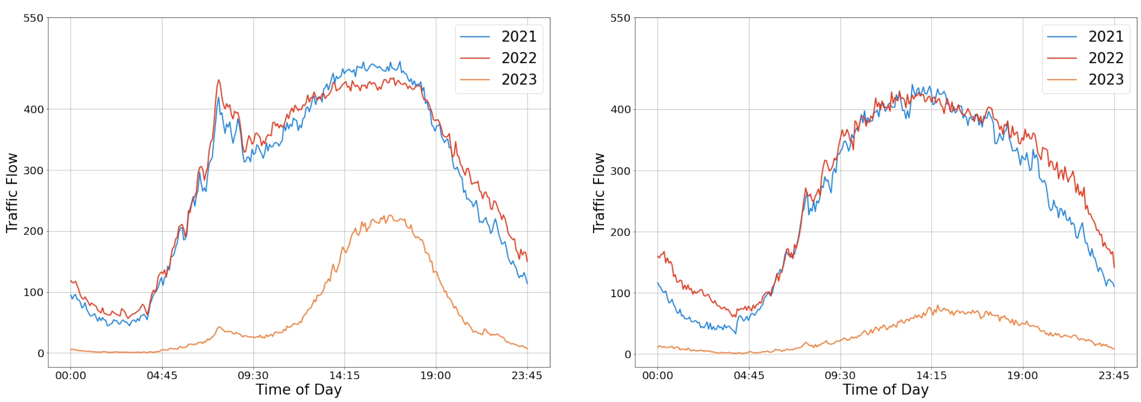

(a) Traffic flow Variation on Weekday (b) Traffic flow Variation on Weekend

Figure 12: (a) and (b) show the variation of traffic flow in one day on Weekday and Weekend, respectively. The color represents the traffic flow in different years.